JOURNAL OF AGRICULTURAL AND FOOD CHEMISTRY

Biotechnology and Biological Transformations

Enantioselective catabolism of napropamide chiral enantiomers in Sphingobium sp. A1 and B2

Jun-Wei Huang, Dian Chen, Xiao-Kun Cheng, Gui-Ping Liu, Guo-xiang Wang, and Jian-Dong Jiang

J. Agric. Food Chem., **Just Accepted Manuscript** • DOI: 10.1021/acs.jafc.9b00707 • Publication Date (Web): 28 May 2019

Just Accepted

is published by the American Chemical Society. 1155 Sixteenth Street N.W., Washington, DC 20036

Enantioselective catabolism of napropamide chiral enantiomers in *Sphingobium* sp. A1 and B2

Junwei Huang[a], Dian Chen[a], Xiaokun Cheng[a], Guiping Liu[a], Guoxiang Wang[c], Jiandong Jiang[a,b,*]

[a]Department of Microbiology, Key Lab of Microbiology for Agricultural Environment, Ministry of Agriculture, College of Life Sciences, Nanjing Agricultural University, 210095, Nanjing, China.

[b]Jiangsu Key Lab for Solid Organic Waste Utilization, 210095, Nanjing, China.

[c]Laboratory Centre of Life Science, College of Life Sciences, Nanjing Agricultural University, 210095, Nanjing, China.

Address correspondence to Jian-Dong Jiang, jiang_jjd@njau.edu.cn;

Tel: +86-025-84399726; Fax: +86-025-84396314

Abstract

Napropamide (*N*,*N*-diethyl-2-(1-naphthalenyloxy)propenamide, NAP) is a highly efficient and broad-spectrum amide herbicide. Little is known about the bacterial catabolism of its different enantiomers**.** Here, we report the isolation of two NAP-degrading strains of *Sphingobium* sp., A1 and B2, and the different catabolic pathways of different enantiomers in these two strains**.** Strain A1 di-oxygenated NAP at different positions of the naphthalene ring of different enantiomers, leading to the complete degradation of *R*-NAP, while producing a dead-end product from *S*-NAP. Strain B2 cleaved the amido bonds of both enantiomers, but only the product from *S*-NAP could be further transformed to form α-naphthol and mineralize in strain B2. The degradation rates of *R*-NAP and *S*-NAP in the combination degradation by strain A1 and B2 were 24.8- and 7.5-times that in the single strain degradation by strain B2 or strain A1, respectively, showing enhanced synergistic catabolism between strains A1 and B2. This study provides new insights into the enantioselective catabolic network of the chiral herbicide NAP in microorganisms.

Key words: Synergistic catabolism; Stereospecific; Napropamide; Mineralized consortium

Introduction

Chiral pesticides comprise 28% of the global pesticide market. In China, the proportion of chiral pesticides has increased from 19% during the 1980s to approximately 40% currently.[1, 2] There are 14 classes and 19 major types of herbicides with chiral centers, accounting for a greater proportion in pesticides. Because of the enantiomeric selectivity from the different effects of the enantiomers on target and non-target organisms, different chiral isomers have been reported to show different biological activities, environmental toxicities, and environmental behaviors.[3, 4] For example, the demethylation of (*S*)-dichlorprop methyl in soil is faster than that of (*R*)-dichlorprop methyl, leading to plant phytotoxicity because of the accumulation of the highly herbicidal (*R*)-dichlorprop methyl in the soil.[3] Some chiral herbicides show the opposite physiological effects.[4] For instance, the *R*-enantiomer of the herbicide diclofop is effective in weed control, while the *S*-enantiomer has no weeding effects but shows more toxicity toward algae than the *R*-enantiomer.[5, 6] The microbial community is one of the important factors affecting the biodegradation of chiral herbicides. Under nonsterilized conditions, more than 99% of the (*R*)- and (*S*)-indoxacarb are dissipated after 75 days of incubation in acidic soil. However, only 5-10% of the initial concentration of (*R*)- and (*S*)-indoxacarb are degraded after 75 days of incubation in sterilized acidic soil.[7] Moreover, *R*- and *S*-enantiomers can be inter-converted by soil microorganisms.[8, 9] (*S*)-indoxacarb had a significantly higher inversion rate to (*R*)-indoxacarb than its antipode in alkaline soil.[7] Because most of the chiral pesticides are chemically synthesized in racemate for use, they inevitably release all isomers into the

environment, despite their activity and toxicity. Consequently, there is an increasing concern of the pollution risk of different isomers of chiral pesticides in the environment.[10] The environmental fate of different isomers, especially their catabolism by microorganisms, needs extensive investigation.

Napropamide (*N*,*N*-diethyl-2-(naphthalen-1-yloxy)propanamide) is a selective systemic amide herbicide used in soils to control several annual grasses and broad-leaved weeds.[11] Napropamide (NAP) is characterized by its efficiency and broad spectrum and selectivity,[11, 12] and it is also found in formulations with other pesticides such as monolinuron, nitralin, simazine, trifluralin, tefluthrin, and tebutam. NAP is a typical chiral herbicide and contains two enantiomers, *R*-NAP and *S*-NAP (Figure S1). Because the chemically synthesized racemic NAP (*Rac*-NAP) is commonly used, both enantiomers enter the environment through point and non-point sources and are distributed in water, soil, sediment and biota.[13] The NAP concentrations detected in the environment range from 0.1 to 0.46 mg/kg.[14, 15] A recent study showed that *R*-NAP had the strongest herbicidal activity, followed by *Rac*-NAP, while *S*-NAP was the weakest. The inhibition effect of *R*-NAP on the root growth of *Echinochloa crusgalli* L. was 9.4 times higher than that of *S*-NAP at the concentration of 0.05 mg/L.[16] Meanwhile, the toxicity of *S*-NAP toward *Microcystis aeruginosa* (EC_{20}<0.1 mg/L) was notably higher than that of *R*-NAP (EC_{20}= 0.1-1.0 mg/L).[16] The molecular docking of NAP enantiomers with the thyroxine receptor (TR) showed that *S*-NAP combined more closely with TR, leading to higher toxicity toward organisms.[16] Therefore, *S*-NAP tends to cause a much more serious threat to ecological systems than *R*-NAP, although both of them are negative to ecosystems. Although microbial degradation has been recognized as the key pathway for the dissipation of NAP from the environment,[17] NAP catabolism via microorganisms has not been extensively studied. *Bacillus* sp. LGY06

is the only pure strain reported to be capable of degrading *Rac*-NAP. However, the complete catabolic pathway of *Rac*-NAP in strain LGY06 has not been elucidated.[18] Moreover, the enantioselective catabolism of the two enantiomers of NAP has never been studied.[18]

In this study, the different catabolic efficiencies and pathways of the two enantiomers of *Rac*-NAP in the two strains of *Sphingobium* sp. A1 and B2 isolated from a *Rac*-NAP-contaminated soil were systematically studied. The enantioselective catabolism of different NAP chiral isomers in strains A1 and B2 was found, and these strains could use complementary pathways to enhance the degradation of *Rac*-NAP and synergistic catabolism to accelerate the degradation of *Rac*-NAP. Our study provides new insights into the enantioselective catabolic network of chiral NAP in microorganisms.

Materials and Methods

1. Chemical reagents, primers, and media

Rac-NAP (99.7%) was purchased from Shanghai Pesticide Research Institute Co., Ltd. (Shanghai, China). Methanol (chromatography grade) and acetic acid (chromatography grade) were purchased from EMD Millipore corporation (Darmstadt, Germany). The other reagents used in this study were commercially available. Luria-Bertani (LB) medium or minimal salt medium (MSM) was used to culture isolated strains at 30°C. Streptomycin (Sm) was added to the medium at 100 mg/L to culture *Sphingobium* species because of their natural resistance to streptomycin.[19]

2. Isolation and characterization of two bacterial strains from a *Rac*-NAP-contaminated soil

Rac-NAP-contaminated soil was collected from Jiangsu Kuaida Agrochemical Co.,

Ltd, China. The isolation of NAP-degrading strains was performed using the traditional enrichment method as previously described with minor modifications.[20] *Rac*-NAP (0.2 mM) was provided as the sole carbon source in MSM for enrichment. Colonies selected from the enrichment were checked for their capacities to degrade *Rac*-NAP via a UV-Visible Spectrophotometer (UV-2450, Shimadzu, Japan) and high-performance liquid chromatography (HPLC, UltiMate 3000 RSLC, Thermo Fisher Scientific, America) with a C_{18} reversed-phase column (4.6 × 250 mm, 5 μm). The separation conditions of the HPLC were as follows: the mobile phase was a mixed solution of methanol: water: acetic acid (75:24:1, v:v:v), the flow rate was 0.8 mL/min, the column temperature was 30°C, the detection wavelength was 250 nm, and the injection volume was 20 μL.[21] All experiments were performed in triplicate. Two strains termed A1 and B2, capable of degrading R-NAP and/or S-NAP, were finally isolated and purified. The isolates were identified based on their morphological, physiological and biochemical properties as well as 16S rRNA gene analysis. The primers 27F (5'-agagtttgatcmtggctcag-3') and 1492R (5'-tacggytaccttgttacgactt-3') were used to amplify the nearly complete 16S rRNA gene. The sequenced 16S rRNA gene sequences of strains A1 and B2 were deposited in the GenBank database under the accession numbers MK411213 and MK447612, respectively.

3. Chiral separation and identification

The enantiomers of *Rac*-NAP were separated using the Shimadzu LC-20AT HPLC system (Shimadzu, Japan). The CHIRALPAK IC (Daicel Corp., Japan) was used as the separation column (4.6 × 150 mm, 5 μm), and the mobile phase was hexane: isopropanol (80:20, v:v) at a flow rate of 1.0 mL/min. The detection wavelength and temperature were 231 nm and 35°C, respectively. The electronic circular dichroism

148 (ECD) spectra of the NAP enantiomers were recorded using a circular dichroism
149 spectropolarimeter J-810 (JASCO Company, Japan) with methanol as the solvent under
150 a wavelength range of from 200 to 400 nm.[22] The ECD plots of *R*-NAP and *S*-NAP
151 were simulated using SpecDis software.[23] The average map was obtained by the
152 Boltzmann-weighted average method and then was compared with the experimental
153 ECD spectrum to determine the absolute configuration.[24-26]
154
155 4. Synergistic catabolism via the combination of strains A1 and B2
156 Strains A1 and B2 were separately cultured in LB medium at 30°C until the mid-log
157 phase. The cells were pelleted by centrifugation at 8000 × g for 10 min and then were
158 washed twice with sterilized H_2O. Strain A1, strain B2 or the combination of strains A1
159 and B2 (cell number 1:1) were inoculated to MSM with 0.2 mM *Rac*-NAP (0.1 mM *R*-
160 NAP plus 0.1 mM *S*-NAP), 0.2 mM *R*-NAP or 0.2 mM *S*-NAP, respectively, at a final
161 concentration of OD_{600} = 0.1. All treatments were incubated at 30°C and 160 rpm.
162 Samples (500 μL) were collected from each treatment at regular intervals and then were
163 mixed with an equal volume of methanol and completely vortexed for 2 min. After
164 centrifugation at 15,000 × g for 3 min, the concentration of each added substrate (*Rac*-
165 NAP, *R*-NAP, and *S*-NAP) in the supernatant was determined using HPLC analysis.
166 Cell growth was determined via OD_{600} measurement. Inoculation with sterilized strain
167 A1 or B2 cells under the same conditions was used as the negative control. All the
168 experiments were performed in triplicate.
169
170 5. Metabolic analysis and identification
171 Strain A1 or strain B2 was incubated in MSM containing 0.2 mM *R*-NAP or *S*-NAP
172 at an initial OD_{600} = 0.1. A sample (1 mL) of the *S*-NAP degradation by strain A1 was

collected at 48 h, while other samples (1 mL) were collected at 6 h. Each collected sample was mixed with an equal methanol volume. After filtration using a 0.22-μm membrane (Millipore, USA), the metabolites were identified using HPLC and liquid chromatography-tandem mass spectrometry (LC-MS/MS). For the HPLC-MS/MS analysis, the HPLC system (Shimadzu, Japan) was connected to a TripleTOF 5600 mass spectrometer (AB SCIEX, American) that was equipped with an electrospray ionization (ESI) probe. The HPLC column was a Kinetex C_{18} (100 mm × 2.1 mm, particle size 2.6 μm). The mobile phase consisted of solvents A (ultrapure water) and B (methanol) with a gradient program that started by maintaining 30% B for 3 min, followed by increasing to 75% B from 3 to 15 min, maintaining 75% B from 15 to 30 min, and then returning to 30% B within 5 min. The flow rate was 0.2 mL/min. The injection volume was 10 μL, and the compounds were first ionized in negative or positive polarity based on their features.

To collect and purify compound 1, strain A1 was cultured and harvested according to the method of Chen et al.[27] The cells were inoculated into MSM medium supplemented with 0.2 mM *S*-napropamide with an initial OD_{600} of 2.0. The cultures were shaken in an incubator at 180 rpm and 30°C. The crude extract of compound 1 was collected as described previously when the substrate was completely degraded.[28] The crude extract of compound 1 was purified using a silica gel column using petroleum ether:acetone (35:1 to 10:1, v/v) as an eluent, followed by elution with acetone to yield compound 1. ^{1}H nuclear magnetic resonance (NMR) (δ), ^{1}H-^{1}H correlation spectroscopy (COSY), heteronuclear single quantum coherence (HSQC), heteronuclear multiple bond correlation (HMBC), and nuclear Overhauser effect spectroscopy (NOESY) data (δ) were measured in Acetone-d6 at 400 MHz, and ^{13}C NMR data (δ) were measured in Acetone-d6 at 100 MHz using Bruker Avance spectrometers (Bruker

BioSpin GmbH, Beijing, China).

6. Cell-free extract preparation and amidohydrolase activity assay in strain B2

Strain B2 cells were grown in 100 mL of LB medium containing 100 mg/L of Sm for 12 h. After centrifugation at 8000 × g for 10 min, the cells were washed twice with deionized water and resuspended in 15 mL of 50 mM phosphate buffer (Na_2HPO_4/NaH_2PO_4, pH 7.4) and disrupted via sonication (Ultrasonic Cell Crusher, Thermo Fisher Scientific, USA). The disrupted cell suspension was centrifuged at 14,000 × g at 4°C for 30 min, and the supernatant was used as the cell-free extract for the amidohydrolase activity assay. A denatured crude enzyme via boiling was prepared as the negative control. The standard enzymatic reaction was performed as previously described with minor modifications.[27] The reaction was stopped by boiling for 1 min. The amidohydrolase activity toward the two enantiomers of NAP was determined using HPLC analysis. One unit of activity (U) was defined as the amount of enzyme that catalyzed the hydrolysis of 1 μmol of *R*-NAP or *S*-NAP per minute. Specific activity was expressed as units per milligram of cell-free extract. The kinetic parameters K_m and V_{max} were calculated using the substrates within a concentration range of 0.1 -1 mM. All the experiments were performed in triplicate.

Results

1. Isolation and identification of two NAP-degrading strains A1 and B2

When the enrichment was subcultured for three rounds, the 0.2 mM *Rac*-NAP in the enrichment nearly disappeared as detected by UV-Visible spectroscopy (Figure 1A). The enrichment was diluted and plated onto MSM agar containing 1 mM *Rac*-NAP at 30°C. Only four morphologically different colonies appeared on the plates after 5 days

of incubation. These four distinct colonies were selected and checked for their capacities to degrade NAP; only two strains, designated A1 and B2, were found to be capable of degrading NAP. Strains A1 and B2 were both strictly aerobic, Gram-negative and rod-shaped. Strain A1 was approximately 1.3-1.6 μm in length and 0.6-0.7 μm in width, and strain B2 was approximately 1.3-1.7 μm in length and 0.6-0.7 μm in width. Strain A1 was determined to be related to the *Sphingobium* species lineage and was closely clustered with *Sphingobium hydrophobicum* $C1^T$ and *Sphingobium xenophagum* NBRC 107872^T, with 16S rRNA gene identities of 99.65% and 99.57%, respectively. The 16S rRNA gene sequence of strain B2 shared 99.93% and 99.86% identities with those of *Sphingobium xenophagum* NBRC 107872^T and *Sphingobium hydrophobicum* $C1^T$, respectively. Based on the above phenotypic characteristics and phylogenetic analyses, strains A1 and B2 were finally identified as two different species of the genus *Sphingobium*. Interestingly, neither of the two isolates could mineralize *Rac*-NAP, while the combination of strains A1 and B2 enhanced degradation of 0.2 mM *Rac*-NAP (Figure 1B).

2. Chiral separation of the two enantiomers of NAP

Rac-NAP was separated by the CHIRALPAK IC (IC00CD-NA012) column of the Shimadzu LC-20AT HPLC system, and two peaks with a retention time of 4.8 min (peak 1) and 6.7 min (peak 2) appeared in the chromatogram (Figure S3). The compounds corresponding to peaks 1 and 2 were collected, and the solvent was removed using rotary evaporation to obtain the pure enantiomers (ee > 99%). The experimental ECD spectra of peak 1 was consistent with the calculated ECD spectra of *R*-NAP and experimental ECD spectra of peak 2 was consistent with the calculated ECD spectra of *S*-NAP. Based on these results, the two compounds corresponding to

peaks 1 and 2 respectively were identified as *R*-NAP and *S*-NAP. (Figure 2).

3. Catabolism of NAP via strains A1 and B2

Strain A1 could use *R*ac-NAP and *R*-NAP as the sole carbon source for growth in MSM (Figure S4A), while strain B2 could not use *R*/*S*/*R*ac-NAP for growth (Figure S4B). Strain A1 completely degraded 0.2 mM *R*-NAP and *S*-NAP over 12 and 108 h, respectively, showing a degrading preference to *R*-NAP (Figure 3A). In contrast to strain A1, strain B2 completely degraded 0.2 mM *S*-NAP over 7 h, while no obvious degradation of *R*-NAP was observed during this time (Figure 3B). Strain B2 showed a weak *R*-NAP degradation ability, and it degraded 49.8% of the 0.2 mM *R*-NAP over 156 h when the cells were inoculated at OD_{600} =2.0 (Figure 3D). The combination of strains A1 and B2 completely degraded 0.2 mM *Rac*-NAP, *R*-NAP or *S*-NAP over 6, 12 and 12 h (Figure 3C), and the degrading efficiencies were higher than those of the single strain. Although the inoculated cell numbers of strain A1/strain B2 in the combination degradation were one-half of that in the single strain degradation, the degradation rates of *R*-NAP and *S*-NAP in the combination degradation were 24.8- and 7.5-times that in the single strain degradation by strain B2 or strain A1, respectively. Additionally, the degradation rate of *Rac*-NAP in the combination degradation was 13.4- or 1.2-times that in the single strain degradation by strain A1 or strain B2, respectively. These data showed enhanced synergistic catabolism between strains A1 and B2.

4. Proposed metabolic pathways of *R*-NAP and *S*-NAP in strain A1 and strain B2

HPLC analysis of samples collected at various times during the degradation of *Rac*-NAP, *R*-NAP or *S*-NAP by strain A1 or strain B2 showed that the decrease in the substrates was accompanied by the appearance of new peaks (metabolites) (Figure 4).

In strain A1, when *Rac*-NAP was used as the substrate, two peaks (Retention time (RT)=4.1 min and 4.7 min) gradually increased and then remained unchanged. For *R*-NAP, two peaks (RT=4.1 min and 6.4 min) occurred at the beginning, and the peak at RT=6.4 min finally disappeared. For *S*-NAP, a peak at RT= 4.7 min (compound 1) mainly accumulated; a small peak at RT=4.1 min was also found (Figure 4A, B and C).

In strain B2, when *Rac*-NAP or *S*-NAP was used as the substrate, two peaks (RT= 7.2 min and 9.4 min) gradually increased, and the peak with RT=7.2 min finally decreased, showing *S*-NAP could be transformed to a metabolite (RT=7.2 min) via the intermediate (RT=9.4 min). For *R*-NAP, no peak at RT=7.2 min formed, and a peak at RT=9.4 min was very small and could not be further degraded (Figure 4D, E and F). Additionally, the metabolite (RT=4.7 min) (compound 1) produced from *S*-NAP by strain A1 could be further transformed to an end-product (RT=3.8 min) by strain B2 (Figure S5).

The two metabolites (RT=4.1 min and 6.4 min) produced from *R*-NAP by strain A1 were identified by HPLC-MS/MS as (*R*)-*N*,*N*-diethyl-2-hydroxypropanamide and (1*R*,2*S*)-1,2-dihydronaphthalene-1,2-diol, with molecular ion peaks $[M+H]^+$ at *d* 146.11 and 163.06, respectively (Figure 5A, C). The metabolite (RT=4.7 min) was identified as (*S*)-2-(((2*S*,3*S*)-2,3-dihydroxy-2,3-dihydronaphthalen-1-yl)oxy)-*N*,*N*-diethylpropanamide at a peak of *m/z* 304.15 and fragments at *m/z* 177.06 (loss of $C_7H_{14}NO$ from 304.15) and *m/z* 159.04 (loss of H_2O from 177.06) (Figure 5B).

The metabolite (RT=9.4 min) produced by strain B2 was identified as *R*-2-(1-naphthalenyloxy)-propanoic acid or *S*-2-(1-naphthalenyloxy)-propanoic acid at a peak of *m/z* 217.10 and its fragments under ionization conditions were at *m/z* 171.08 (loss of CHO_2 from 217.10), *m/z* 143.05 (loss of C_2H_4 from 171.08) and *m/z* 127.05 (loss of O from 143.05) (Figure 5D). The metabolite (RT=7.2 min) was identified as naphthol,

298 with a molecular ion peak $[M+H]^+$ at 145.06 and a fragment at *m/z* 127.05 (loss of HO
299 from 145.06) (Figure 5E). Another metabolite (RT=3.8 min) was identified as (*S*)-2-
300 (((2*S*,3*S*)-2,3-dihydroxy-2,3-dihydronaphthalen-1-yl)oxy)propanoic acid with a peak at
301 *m/z* 249.07 and a fragment at *m/z* 177.06 (loss of $C_3H_5O_2$ from 249.07) (Figure 5F).
302 According to the results of the HPLC and HPLC-MS/MS analyses, we speculated on
303 the metabolic pathways of *S*-NAP and *R*-NAP in strains A1 and B2. In strain B2, the
304 amide bond of *S*-NAP was broken to generate *S*-2-(1-naphthalenyloxy)-propanoic acid
305 (*S*-NP) and diethylamine. The ether bond of *S*-NP was then cleaved to form *α*-naphthol,
306 which finally entered the tricarboxylic acid (TCA) cycle (Figure 6B, green). Meanwhile,
307 for *R*-NAP, the amide bond was also broken to generate *R*-2-(1-naphthalenyloxy)-
308 propanoic acid (*R*-NP) and diethylamine, but none of them could be further transformed
309 (Figure 6A, green). In strain A1, *S*-NAP slowly transformed to the end-products (*S*)-2-
310 (((2*S*,3*S*)-2,3-dihydroxy-2,3-dihydronaphthalen-1-yl)oxy)-*N*,*N*-diethylpropanamide
311 and (*S*)-*N*,*N*-diethyl-2-hydroxypropanamide (Figure 6B, orange). Although (*S*)-2-
312 (((2*S*,3*S*)-2,3-dihydroxy-2,3-dihydronaphthalen-1-yl)oxy)-*N*,*N*-diethylpropanamide
313 could not be further transformed by strain A1, it could be further transformed to
314 (1*R*,2*S*)-1,2-dihydronaphthalene-1,2-diol (RT=3.8 min) by strain B2 (Figure S5). By
315 contrast, strain A1 could transform *R*-NAP to (*R*)-*N*,*N*-diethyl-2-hydroxypropanamide
316 and (1*R*,2*S*)-1,2-dihydronaphthalene-1,2-diol, which could be further metabolized to
317 CO_2 and H_2O, respectively (Figure 6A, orange).
318
319 5. Structural determination of compound 1 by NMR analysis
320 HRTOF-MS analysis of compound 1 (RT=4.7 min) showed a molecular ion peak at
321 *m/z* = 304.1578 $[M - H]^-$ (Figure 5B), suggesting the molecular formula $C_{17}H_{23}NO_4$,
322 accounting for seven degrees of unsaturation (Figure 7). The ^1H NMR spectrum of

compound 1 showed three aromatic proton signals in an ABC spin system at δ_H 7.18 (1H, dd, J = 8.0, 8.0 Hz), 6.82 (1H, d, J = 8.0 Hz), and 6.75 (1H, d, J = 8.0 Hz), corresponding to a 1,2,3-trisubstituted benzene ring (Figure S6). It also showed resonances for a disubstituted double bond at δ_H 6.36 (1H, dd, 9.6, 2.4) and 5.83 (1H, dt, 9.6, 2.0), and two NCH_2CH_3 groups at 3.33 (2H, m), 1.05 (3H, t, J = 6.8 Hz), 3.48 (2H, m), and 1.13 (3H, t, J = 6.8 Hz). The resonances at δ_H 5.05 (1H, d, J = 3.2 Hz) and 4.40 (1H, m) were assigned to the two vicinal oxymethine groups and those at δ_H 5.16 (1H, q, J = 6.4 Hz) and 1.52 (3H, d, J = 6.4) to the mutually coupled oxymethine and methyl groups (Table 1), respectively. The ^{13}C NMR data for compound 1 showed the presence of 17 carbons comprising an amide carbonyl, eight aromatic/olefinic carbons, and eight aliphatic carbons (Figure S7). The ^{1}H and ^{13}C NMR spectroscopic data were similar to those of napropamide except for the replacement of the resonances of a double bond at C-6/C-7 in the napropamide by signals for a vicinal diol in compound 1 (Figure S8, S9). HMBC from H-4 (δ_H 6.75) to C-6 (δ_C 63.7) confirmed this assignment (Figure S10). The relatively small coupling constant (J = 3.2 Hz) between H-6 (δ_H 5.05) and H-7 (δ_H 4.40) suggested that they were oriented on the same side of the cyclohexene ring. This deduction was supported by an NOE correlation of H-6/H-7 (Figure S11). Based on these data, compound 1 was identified as 2-((5,6-dihydroxy-5,6-dihydronaphthalen-1-yl)oxy)-*N*,*N*-diethylpropanamide.

6. Amidohydrolase activity in strain B2

The metabolic pathways of NAP in strain B2 showed the presence of amidohydrolase. HPLC results confirmed that the cell-free extract of strain B2 could transform *S*-

NAP/*R*-NAP to *S*-NP/*R*-NP (Figure S12). The kinetic parameters and catalytic efficiency (k_{cat}/K_m) of the crude amidohydrolase extracted from strain B2 are summarized in Table 2. The amidohydrolase from strain B2 showed a catalytic preference for *S*-NAP compared with that for *R*-NAP. It transformed 29% of 0.2 mM *S*-NAP within 10 min when 12 μg of cell-free extract was used, while it only transformed 18% of 0.2 mM *R*-NAP within 72 h when 600 μg of cell-free extract was used.

Discussion

Napropamide (NAP) belongs to the amide herbicide family. It is a chiral herbicide and among the most commonly used pre-emergence herbicides for fruits, vegetables and crops to control broadleaf weeds.[29] NAP is polar and slightly soluble in water, and easily passes into the tissues of organisms and soil layer,[30] showing a threat to the safety of drinking water. Although previous investigations have shown that NAP in the environment was mainly eliminated by microbial transformation, only a few published studies regarding NAP microbial degradation have been reported and the catabolism of the different NAP chiral isomers has not been investigated. In this study, we isolated two *Sphingobium* species from a *Rac*-NAP-contaminated soil. Neither strain A1 nor strain B2 or the combination of strains A1 and B2 could mineralize *Rac*-NAP, but the combination of strains A1 and B2 could enhance the degradation of *Rac*-NAP, indicating synergistic degradation of the two enantiomers of NAP by strains A1 and B2.

The degradation of *R*/*S*-NAP by strain A1 or strain B2 was shown to be enantioselective. The degradation rates of *S*/*R*-NAP by strain A1 and strain B2 were also different. Under the same inoculum, the degradation rate of *R*-NAP by strain A1 was 12-times faster than that of *S*-NAP, while strain B2 completely degraded 0.2 mM

371 *S*-NAP within 7 h and showed no significant degradation of *R*-NAP. The
372 enantioselective degradation of the enantiomers might be because of the different
373 spatial structures of the different enantiomers, causing a different distance between the
374 catalytic site of the degrading enzymes and target group of enantiomers to be
375 catalyzed.[26] Nevertheless, the specific mechanism involved needs further research. For
376 example, Wen et al. showed that the main reason for the selectivity of *Aspergillus niger*
377 lipase (ANL, EC3.1.1.3) to 2,4-dichlorprop-methyl was enzymatic conformation and
378 the binding pattern of 2,4-dichlorprop-methyl to this enzyme.[31]

379 Strain A1 transformed *R*-NAP to (*R*)-*N*,*N*-diethyl-2-hydroxypropanamide and
380 (1*R*,2*S*)-1,2-dihydronaphthalene-1,2-diol, and the latter metabolite could be completely
381 mineralized. However, strain A1 could only transform *S*-NAP to the end-products (*S*)-
382 2-(((2*S*,3*S*)-2,3-dihydroxy-2,3-dihydronaphthalen-1-yl)oxy)-*N*,*N*-diethylpropanamide
383 and (*S*)-*N*,*N*-diethyl-2-hydroxypropanamide. Interestingly, strain B2 only transformed
384 *R*-NAP to the end-products diethylamine and *R*-NP but mineralized *S*-NAP via the
385 intermediate *S*-NP. These results showed that strain A1 preferred to degrade *R*-NAP,
386 while strain B2 preferred to degrade *S*-NAP, and strains A1 and B2 complemented each
387 other to enhance the degradation of both enantiomers. The reason that one single strain
388 has not evolved the mineralizing pathways for both enantiomers might be that the i)
389 evolution of complementary pathways for both enantiomers is difficult and needs a long
390 time; ii) distribution of metabolic pathways in different strains is beneficial to hosts,
391 and the toxic effects of NAP, as well as its metabolites, are reduced in a single strain;
392 iii) the degradation efficiency of NAP is enhanced via synergism; and iv) the ecological
393 balance among the bacterial consortium is maintained.[32]

394 During the degradation of *R*/*S*-NAP via a single strain A1 or strain B2, end-products
395 were produced. However, no end-product was detected in the enrichment, suggesting

that some unisolated strains in the enrichment could degrade these end-products. Organic pollutants synergistically degraded by bacterial consortia are common.[33, 34] For example, the combination of the *Diaphorobacter* sp. strain LR2014-1 with *Achromobacter* sp. strain ANB-1 resulted in enhanced degradation of the phenylurea herbicide linuron.[35]

Notably, the degradation of naphthol, the downstream product of *S*-NAP, by strain B2 in MSM was greatly enhanced by the addition of glucose or LB (data not shown). This phenomenon was similar to that mentioned by Teramoto et al.[36] We speculated the presence of a regulator that can interact with glucose or its metabolite regulates naphthol degradation in strain B2.

Taken together, we isolated two strains of *Sphingobium* sp., A1 and B2, which showed different preferences for the catabolism of the different NAP enantiomers. Strains A1 and B2 could complement each other to synergistically enhance the catabolism of both enantiomers. Our study provides new insights into the enantioselective catabolism of chiral NAP in microorganisms.

Abbreviations

NAP: Napropamide; *Rac*-NAP: racemic NAP or *Rac*-napropamide; TR: thyroxine receptor; LB: Luria-Bertani medium; MSM: minimal salt medium; Sm: Streptomycin; HPLC: high-performance liquid chromatography; ECD: electronic circular dichroism; OD_{600}: optical cell density at 600 nm; HPLC-MS/MS: high-performance liquid chromatography-tandem mass spectrometry; ESI: electrospray ionization; *S*-NP: *S*-2-(1-naphthalenyloxy)-propanoic acid; *R*-NP: *R*-2-(1-naphthalenyloxy)-propanoic acid; NMR: nuclear magnetic resonance; ^{1}H-^{1}H COSY: ^{1}H-^{1}H correlation spectroscopy;

HSQC: heteronuclear single quantum coherence; HMBC: heteronuclear multiple bond correlations; NOESY: nuclear Overhauser effect spectroscopy; RT: retention time; TCA cycle: tricarboxylic acid cycle; ANL: *Aspergillus niger* lipase.

Acknowledgment

This work was supported by the grant from the National Natural Science Foundation of China (grant no. 31870087) and the Postgraduate Research Practice Innovation Program of Jiangsu Province (grant no. KYCX17_0658).

Notes

The authors declare no competing financial interest.

References

1. Ye, J.; Wu, J.; Liu, W. P., Enantioselective separation and analysis of chiral pesticides by high-performance liquid chromatography. *Trac-Trend Anal Chem*. **2009**, *28*, 1148-1163.

2. Liu, W. P.; Ye, J.; Jin, M. Q., Enantioselective phytoeffects of chiral pesticides. *J. Agric. Food Chem*. **2009**, *57*, 2087-2095.

3. Lewis, D. L.; Garrison, A. W.; Wommack, K. E.; Whittemore, A.; Steudler, P.; Melillo, J., Influence of environmental changes on degradation of chiral pollutants in soils. *Nature*. **1999**, *401*, 898-901.

4. Liu, W. P.; Gan, J. Y.; Schlenk, D.; Jury, W. A., Enantioselectivity in environmental safety of current chiral insecticides. *Proc. Natl. Acad. Sci. USA*. **2005**, *102*, 701-706.

443 5. Muller, T. A.; Kohler, H. P. E., Chirality of pollutants - effects on metabolism and
444 fate. *Appl. Microbiol. Biotechnol.* **2004**, *64*, 300-316.
445 6. Ye, J.; Zhao, M. R.; Niu, L. L.; Liu, W. P., Enantioselective environmental
446 toxicology of chiral pesticides. *Chem. Res. Toxicol.* **2015**, *28*, 325-338.
447 7. Sun, D.; Pang, J.; Qiu, J.; Li, L.; Liu, C.; Jiao, B., Enantioselective degradation and
448 enantiomerization of indoxacarb in soil. *J. Agric. Food Chem*. **2013**, *61*, 11273-11277.
449 8. Buser, H. R.; Muller, M. D.; Poiger, T.; Balmer, M. E., Environmental behavior of
450 the chiral acetamide pesticide metalaxyl: Enantioselective degradation and chiral
451 stability in soil. *Environ. Sci. Technol.* **2002**, *36*, 221-226.
452 9. Muller, M. D.; Buser, H. R., Conversion reactions of various phenoxyalkanoic acid
453 herbicides in soil .1. Enantiomerization and enantioselective degradation of the chiral
454 2-phenoxypropionic acid herbicides. *Environ. Sci. Technol.* **1997**, *31*, 1953-1959.
455 10. Huang, X.; He, J.; Yan, X.; Hong, Q.; Chen, K.; He, Q.; Zhang, L.; Liu, X. W.;
456 Chuang, S. C.; Li, S. P.; Jiang, J. D., Microbial catabolism of chemical herbicides:
457 Microbial resources, metabolic pathways and catabolic genes. *Pestic. Biochem. Physiol.*
458 **2017**, *143*, 272-297.
459 11. Qi, Y. L.; Liu, D. H.; Zhao, W. T.; Liu, C.; Zhou, Z. Q.; Wang, P., Enantioselective
460 phytotoxicity and bioacitivity of the enantiomers of the herbicide napropamide. *Pestic.*
461 *Biochem. Physiol*. **2015**, *125*, 38-44.
462 12. Qi, Y. L.; Liu, D. H.; Sun, M. J.; Di, S. S.; Wang, P.; Zhou, Z. Q., The chiral
463 separation and enantioselective degradation of the chiral herbicide napropamide.
464 *Chirality*. **2014**, *26*, 108-113.

13. Cui, L. E.; Yang, H., Accumulation and residue of napropamide in alfalfa (*Medicago sativa*) and soil involved in toxic response. *J. Hazard. Mater.* **2011**, *190*, 81-86.

14. Walker, A.; Brown, P. A.; Mathews, P. R., Persistence and phytotoxicity of napropamide residues in soil. *Ann. Appl. Biol.* **1985**, *106*, 323-333.

15. Cao, C. F.; Wang, Z.; Urruty, L.; Pommier, J. J.; Montury, M., Focused microwave assistance for extracting some pesticide residues from strawberries into water before their determination by SPME/HPLC/DAD. *J. Agric. Food Chem.* **2001**, *49*, 5092-5097.

16. Xie, J. Q.; Zhao, L.; Liu, K.; Guo, F. J.; Liu, W. P., Enantioselective effects of chiral amide herbicides napropamide, acetochlor and propisochlor: The more efficient *R*-enantiomer and its environmental friendly. *Sci. Total Environ.* **2018**, *626*, 860-866.

17. Walker, A.; Parekh, N. R.; Roberts, S. J.; Welch, S. J., Evidence for the enhanced biodegradation of napropamide in soil. *Pestic. Sci.* **1993**, *39*, 55-60.

18. Zhang, C.; Wu, X. M.; Long, Y. H.; Li, M.; Li, R. Y.; Yin, X. H., Identification and degradation characteristics of a napropamide-degrading bacterium strain. *Chin. J. Appl. Ecol.* **2016**, *27*, 3371-3378.

19. Kaczmarczyk, A.; Vorholt, J. A.; Francez-Charlot, A., Markerless gene deletion system for Sphingomonads. *Appl. Environ. Microbiol.* **2012**, *78*, 3774-3777.

20. Liu, X. M.; Chen, K.; Meng, C.; Zhang, L.; Zhu, J. C.; Huang, X.; Li, S. P.; Jiang, J. D., *Pseudoxanthobacter liyangensis* sp nov., isolated from dichlorodiphenyltrichloroethane-contaminated soil. *Int. J. Syst. Evol. Microbiol.* **2014**, *64*, 3390-3394.

487 21. Yan, X.; Huang, J.; Xu, X.; Chen, D.; Xie, X.; Tao, Q.; He, J.; Jiang, J., Enhanced
488 and complete removal of phenylurea herbicides by combinational transgenic plant-
489 microbe remediation. *Appl. Environ. Microbiol.* **2018**, *84*, e00273-18.
490 22. Xu, Y. X.; Zhang, H.; Zhuang, S. L.; Yu, M.; Xiao, H.; Qian, M. R., Different
491 enantioselective degradation of pyraclofos in soils. *J. Agric. Food Chem.* **2012**, *60*,
492 4173-4178.
493 23. Bruhn, T.; Schaumloffel, A.; Hemberger, Y.; Bringmann, G., Specdis: Quantifying
494 the comparison of calculated and experimental electronic circular dichroism spectra.
495 *Chirality*. **2013**, *25*, 243-249.
496 24. O'Boyle, N. M.; Vandermeersch, T.; Flynn, C. J.; Maguire, A. R.; Hutchison, G. R.,
497 Confab - systematic generation of diverse low-energy conformers. *J. Cheminf.* **2011**, *3*,
498 8.
499 25. Li, L. Z.; Liang, X.; Sun, X.; Qi, X. L.; Wang, J.; Zhao, Q. C.; Song, S. J., Bioactive
500 norditerpenoids and neolignans from the roots of salvia miltiorrhiza. *Org. Biomol.*
501 *Chem.* **2016**, *14*, 10050-10057.
502 26. Zhang, C. L.; Liu, Y. F.; Wang, Y.; Liang, D.; Jiang, Z. B.; Li, L.; Hao, Z. Y.; Luo,
503 H.; Shi, G. R.; Chen, R. Y.; Cao, Z. Y.; Yu, D. Q., Polycycloiridals A-D, four iridal-type
504 triterpenoids with an α-terpineol moiety from *Iris tectorum*. *Org. Lett.* **2015**, *17*, 5686-
505 5689.
506 27. Chen, D. A.; Kong, X. K.; Wu, S. R.; Huang, J. W.; Cheng, X. K.; Jiang, J. D., An
507 esterase Apph for the hydrolysis of 2-(4-aryloxyphenoxy) propionate herbicides in
508 *Sphingobium* sp. strain C3. *Int. Biodeter. Biodegr.* **2019**, *136*, 34-40.

509 28. Chen, X.; Ji, J.; Zhao, L.; Qiu, J.; Dai, C.; Wang, W.; He, J.; Jiang, J.; Hong, Q.;
510 Yan, X., Molecular mechanism and genetic determinants of buprofezin degradation.
511 *Appl. Environ. Microbiol.* **2017**, *83*, e00868-17.
512 29. Cycon, M.; Wojcik, M.; Borymski, S.; Piotrowska-Seget, Z., Short-term effects of
513 the herbicide napropamide on the activity and structure of the soil microbial community
514 assessed by the multi-approach analysis. *Appl. Soil Ecol.* **2013**, *66*, 8-18.
515 30. Biswas, P. K.; Pramanik, S. K.; Mitra, S. R.; Bhattacharyya, A., Persistence of
516 napropamide in/on tea under north-east Indian climatic condition. *Bull. Environ.*
517 *Contam. Toxicol.* **2007**, *79*, 566-569.
518 31. Wen, Y. Z.; Li, C. D.; Fang, Z. H.; Zhuang, S. L.; Liu, W. P., Elucidation of the
519 enantioselective enzymatic hydrolysis of chiral herbicide dichlorprop methyl by
520 chemical modification. *J. Agric. Food Chem.* **2011**, *59*, 1924-1930.
521 32. Crofts, T. S.; Wang, B.; Spivak, A.; Gianoulis, T. A.; Forsberg, K. J.; Gibson, M.
522 K.; Johnsky, L. A.; Broomall, S. M.; Rosenzweig, C. N.; Skowronski, E. W., Shared
523 strategies for β-lactam catabolism in the soil microbiome. *Nat. Chem. Biol.* **2018**, *14*,
524 556-564.
525 33. Sorensen, S. R.; Albers, C. N.; Aamand, J., Rapid mineralization of the phenylurea
526 herbicide diuron by *Variovorax* sp strain SRS16 in pure culture and within a two-
527 member consortium. *Appl. Environ. Microbiol.* **2008**, *74*, 2332-2340.
528 34. Breugelmans, P.; D'Huys, P. J.; De Mot, R.; Springael, D., Characterization of
529 novel linuron-mineralizing bacterial consortia enriched from long-term linuron-treated
530 agricultural soils. *FEMS Microbiol. Ecol.* **2007**, *62*, 374-385.

531 35. Zhang, L.; Hang, P.; Hu, Q.; Chen, X. L.; Zhou, X. Y.; Chen, K.; Jiang, J. D.,
532 Degradation of phenylurea herbicides by a novel bacterial consortium containing
533 synergistically catabolic species and functionally complementary hydrolases. *J. Agric.*
534 *Food Chem.* **2018**, *66*, 12479-12489.
535 36. Teramoto, M.; Harayama, S.; Watanabe, K., Phcs represses gratuitous expression
536 of phenol-metabolizing enzymes in *Comamonas testosteroni* R5. *J. Bacteriol.* **2001**,
537 *183*, 4227-4234.
538
539
540
541
542
543
544
545
546
547
548
549
550
551
552
553
554

555 **Figure captions**

556 Figure 1. UV spectrum scanning of *Rac*-napropamide (*Rac*-NAP) after one-week
557 degradation by the enrichment culture (A) and isolated strain(s) (B). MSM containing
558 0.2 mM *Rac*-napropamide and inoculated with sterilized enrichment culture was used
559 as the control.

560

561 Figure 2. Calculated ECD spectra of configurations *R*-napropamide (red) and *S*-
562 napropamide (blue) were compared with the experimental ECD spectra (black) of peak
563 1 (A) and peak 2 (B) shown in Figure S3.

564

565 Figure 3. Degradation of *Rac*-napropamide (*Rac*-NAP), *R*-napropamide (*R*-NAP) and
566 *S*-napropamide (*S*-NAP) by strain A1 (A), strain B2 (B) and the combination of strains
567 A1 and B2 (C), respectively. Degradation of *R*-NAP by strain B2 with a high amount
568 inoculation (D). Cells of strain A1 or strain B2 were inoculated for individual
569 degradation in 100 mL of MSM at an initial OD_{600} value of 0.1 (A and B) and 2.0 (D),
570 and cells of strain A1 and strain B2 were simultaneously inoculated for a combination
571 degradation in 100 mL of MSM at an initial OD_{600} value of 0.05 for every strain (C).
572 The concentration of *Rac*-napropamide, *R*-napropamide and *S*-napropamide for each
573 treatment was 0.2 mM. The data are expressed as the mean and standard deviation of
574 three replicates.

575

576 Figure 4. HPLC spectral analysis of the metabolites of *Rac*-napropamide (A, D), *R*-

577 napropamide (B, E) and *S*-napropamide (C, F) during the degradation by strain A1 (A,
578 B, C) or strain B2 (D, E, F).
579
580 Figure 5. HPLC-MS/MS analysis of the metabolites during *R*-napropamide or *S*-
581 napropamide degradation by strain A1 or strain B2. Tandem mass spectrometry of
582 metabolites at 4.1 min (A), 4.7 min (B) and 6.4 min (C) produced by strain A1 (see in
583 Figure 4A, 4B and 4C). Tandem mass spectrometry of metabolites at 9.4 min (D), 7.2
584 min (E) and 3.8 min (F) produced by strain B2 (see Figure 4D, 4E, and 4F and Figure
585 S4).
586
587 Figure 6. Proposed metabolic pathways of *R*-napropamide (A) and *S*-napropamide (B)
588 in strain A1 (in orange) or strain B2 (in green). TCA is an abbreviation for tricarboxylic
589 acid cycle.
590
591 Figure 7. Structure of compound 1.
592
593
594
595
596
597
598

599 **Table 1** ^{1}H-NMR and ^{13}C-NMR data of compound 1[a]

NO.	δ_H	δ_C
1		156.8
2	6.82, d (8.0)	114.3
3	7.18, dd (8.0, 8.0)	130.0
4	6.75, d (8.0)	120.9
5		135.0
6	5.05, d (3.2)	63.7
7	4.40, m	70.7
8	5.83, dt (9.6, 2.0)	133.7
9	6.36, dd (9.6, 2.4)	127.0
10		125.5
11	5.16, dd (13.2, 6.4)	73.7
12	1.52, d (6.4)	18.5
13		170.5
14	3.33, m	40.7
15	1.05, t (6.8)	13.0
16	3.48, m	41.8
17	1.13, t (6.8)	14.8

600 [a] ^{1}H NMR data (δ) were measured in Acetone-d_6 at 400 MHz; ^{13}C NMR data (δ) were
601 measured in Acetone-d_6 at 100 MHz.
602
603
604
605
606
607
608
609
610
611
612
613
614
615
616
617
618
619
620
621
622
623

624 **Table 2** Kinetic parameters [a] of crude amidohydrolase extracted from strain B2

Substrate	Specific activity (U/mg)	K_m (μM)	V_{max} (umol/min·mg)
S-napropamide	227.4 ± 3.6	24.6 ± 1.1	336.7 ± 0.4
R-napropamide	3.2 ± 1.9	32.2 ± 0.3	6.4 ± 0.6

625 [a] Kinetic experiments were performed at 30°C in phosphate buffer (50 mM, pH 7.4)
626 with a final volume of 500 μL. The data are expressed as the mean and standard
627 deviation of three replicates.
628
629
630
631
632
633
634
635
636
637
638
639
640
641
642
643
644
645
646
647
648
649
650
651
652
653
654
655
656
657
658
659
660
661
662
663

Figure 1

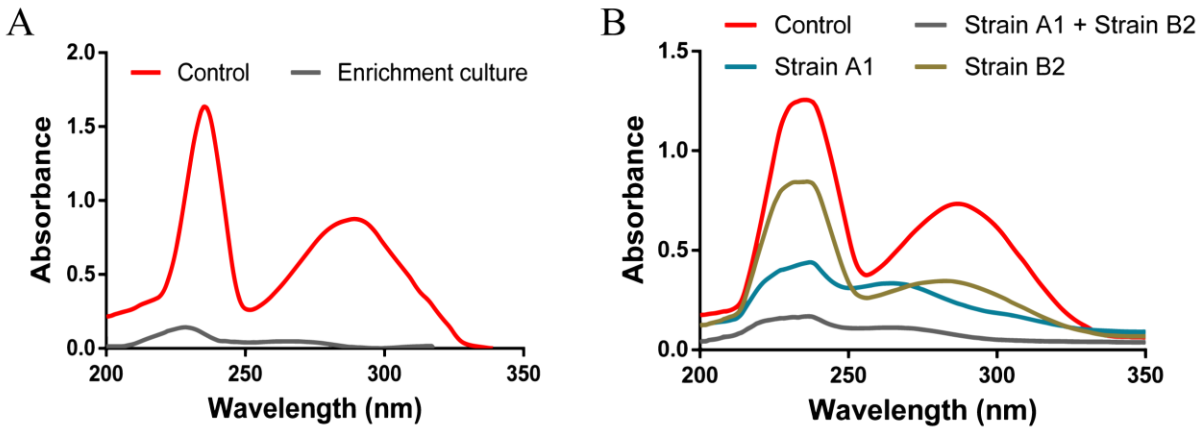

Figure 1. UV spectrum scanning of *Rac*-napropamide (*Rac*-NAP) after one-week degradation by the enrichment culture (A) and isolated strain(s) (B). An MSM containing 0.2 mM *Rac*-napropamide and inoculated with sterilized enrichment culture was used as the control.

Figure 2

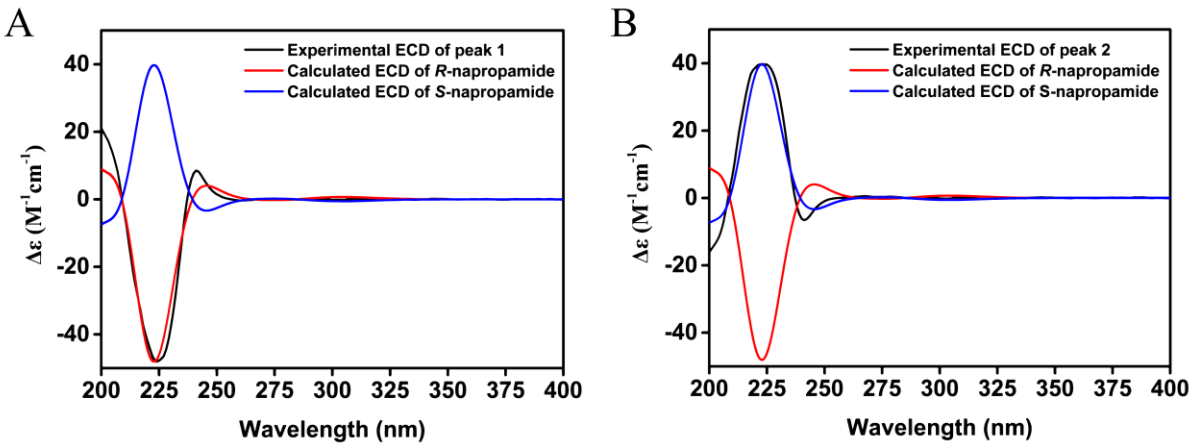

Figure 2. Calculated ECD spectra of configurations *R*-napropamide (red) and *S*-napropamide (blue) were compared with the experimental ECD spectra (black) of peak 1 (A) and peak 2 (B) shown in Figure S3.

Figure 3

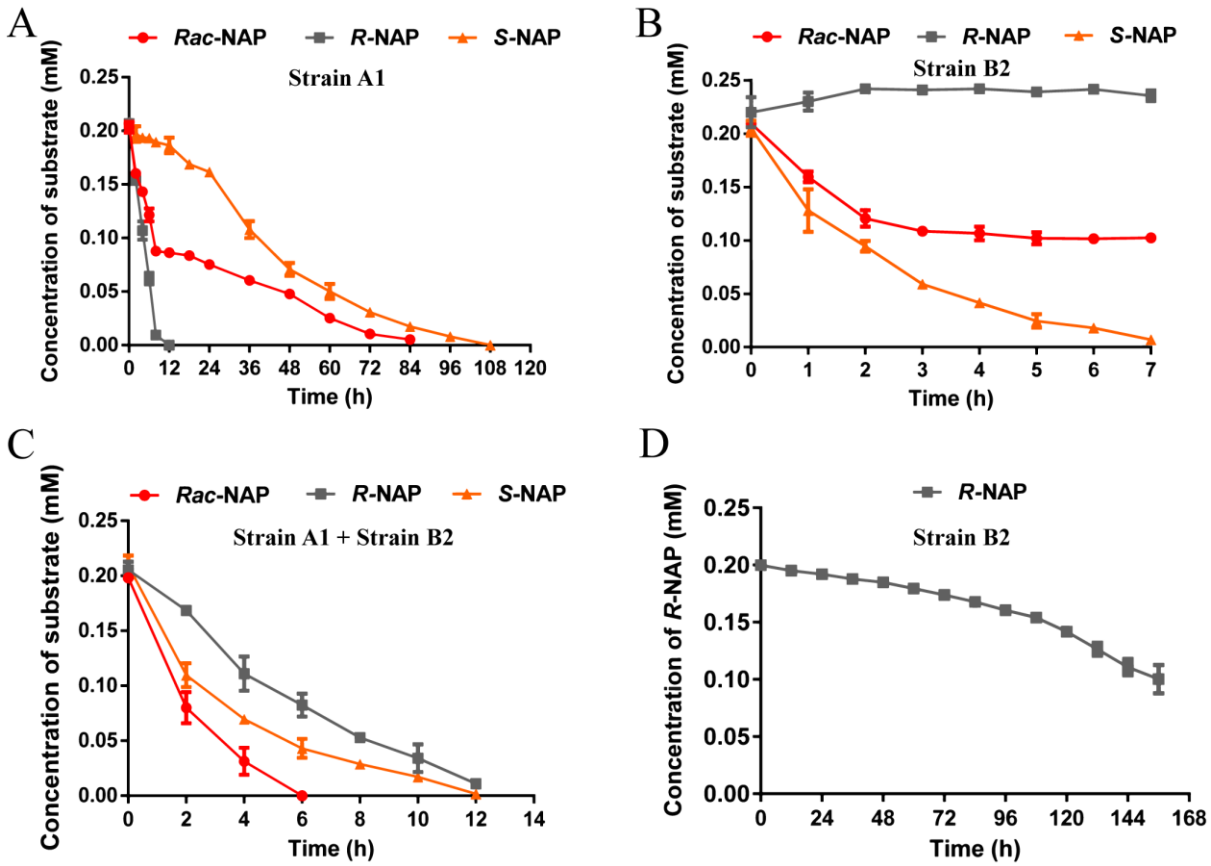

Figure 3. Degradation of *Rac*-napropamide (*Rac*-NAP), *R*-napropamide (*R*-NAP) and *S*-napropamide (*S*-NAP) by strain A1 (A), strain B2 (B) and the combination of strains A1 and B2 (C), respectively. Degradation of *R*-NAP by strain B2 with a high amount inoculation (D). Cells of strain A1 or strain B2 were inoculated for individual degradation in 100 mL of MSM at an initial OD_{600} value of 0.1 (A and B) and 2.0 (D), and cells of strain A1 and strain B2 were simultaneously inoculated for a combination degradation in 100 mL of MSM at an initial OD_{600} value of 0.05 for every strain (C). The concentration of *Rac*-napropamide, *R*-napropamide and *S*-napropamide for each treatment was 0.2 mM. The data are expressed as the mean and standard deviation of three replicates.

Figure 4

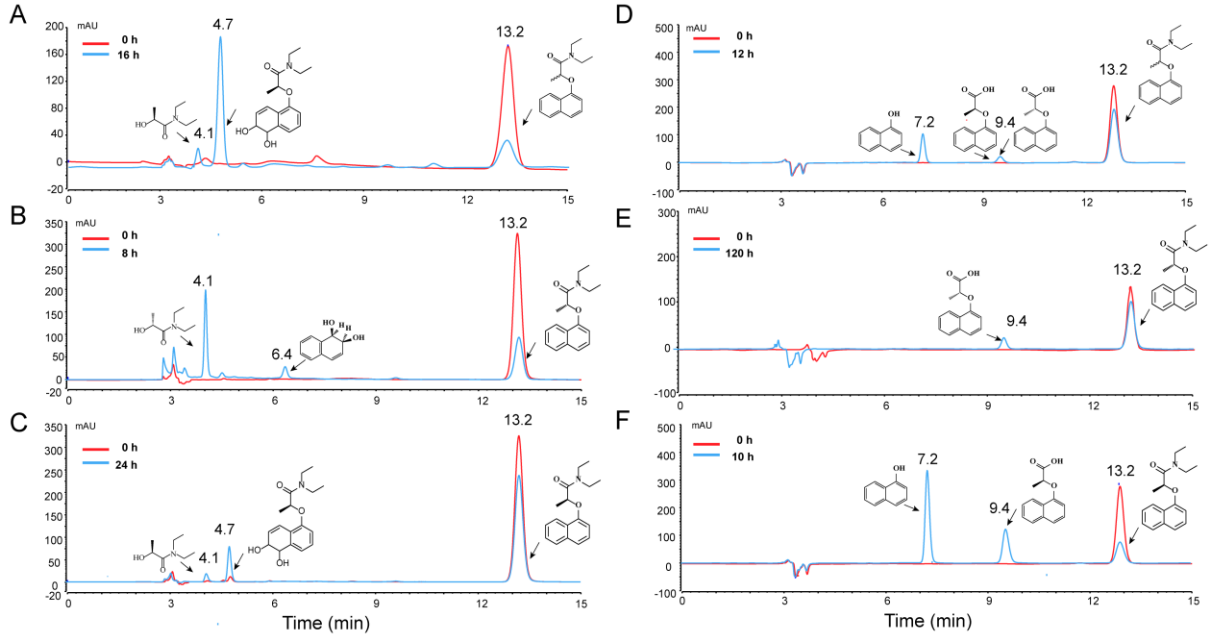

Figure 4. HPLC spectral analysis of the metabolites of *Rac*-napropamide (A, D), *R*-napropamide (B, E) and *S*-napropamide (C, F) during the degradation by strain A1 (A, B, C) or strain B2 (D, E, F).

Figure 5

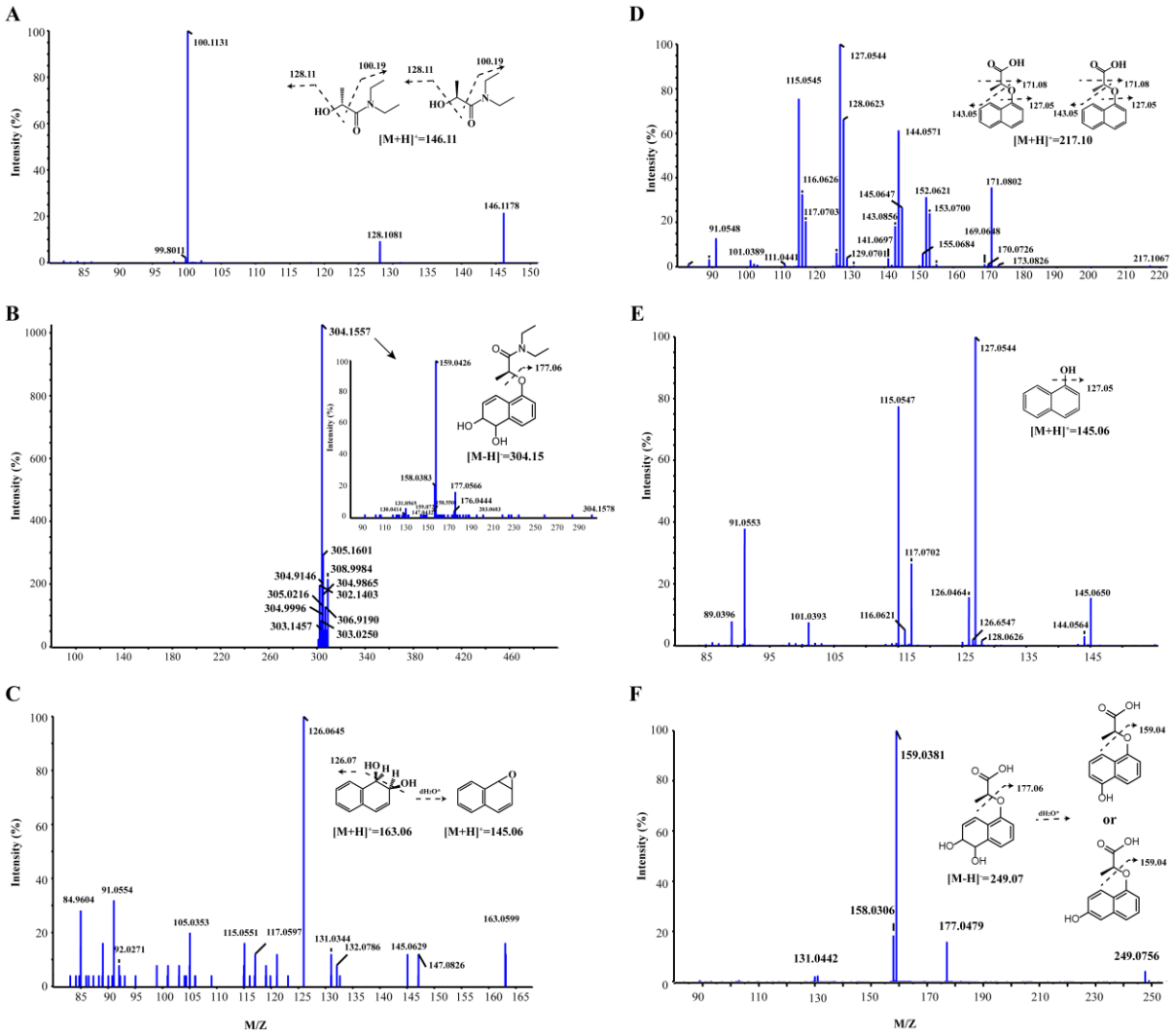

Figure 5. HPLC-MS/MS analysis of the metabolites during *R*-napropamide or *S*-napropamide degradation by strain A1 or strain B2. Tandem mass spectrometry of metabolites at 4.1 min (A), 4.7 min (B) and 6.4 min (C) produced by strain A1 (see in Figure 4A, 4B and 4C). Tandem mass spectrometry of metabolites at 9.4 min (D), 7.2 min (E) and 3.8 min (F) produced by strain B2 (see Figure 4D, 4E, and 4F and Figure S5).

Figure 6

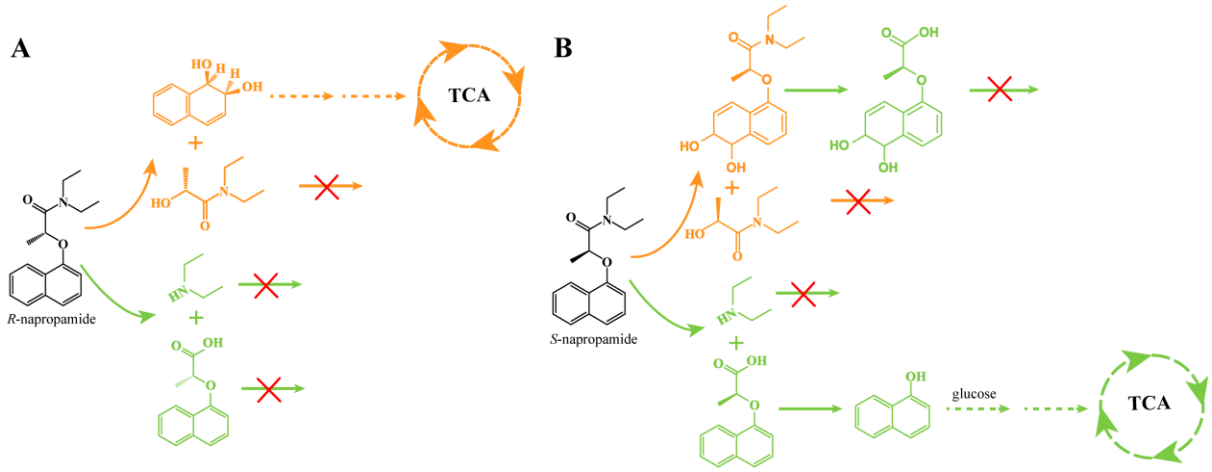

Figure 6. Proposed metabolic pathways of *R*-napropamide (A) and *S*-napropamide (B) in strain A1 (in orange) or strain B2 (in green). TCA is an abbreviation for tricarboxylic acid cycle.

Figure 7

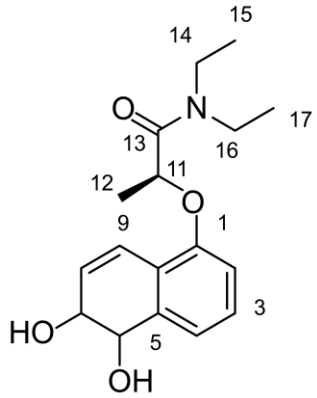

Figure 7. Structure of compound 1.

872 Graphic for table of contents

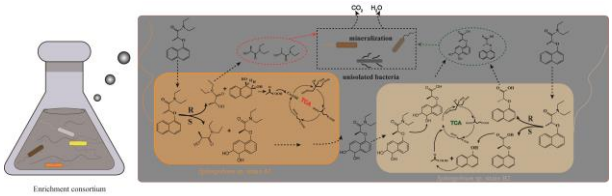

873